IEEE Access
Multidisciplinary | Rapid Review | Open Access Journal

Received May 6, 2019, accepted June 27, 2019, date of publication July 9, 2019, date of current version July 26, 2019.

Digital Object Identifier 10.1109/ACCESS.2019.2927716

A Hybrid Clustering Strategy for Transform Domain Communication System

SHIYONG MA, SU HU, XUEZHANG ZHU, QIUDI TANG, QU LUO, AND YUNFENG ZHOU

National Key Laboratory of Science and Technology on Communications, University of Electronic Science and Technology of China, Chengdu 611731, China

Corresponding author: Su Hu (husu@uestc.edu.cn)

This work was jointly supported by National Key R&D Program of China (No. 2018YFC0807101, No. 2016YFE0123200), National Natural Science Foundation of China (No. 61571082, No. 61701503, No. 61750110527), and National Defense Science and Technology Innovation Project.

ABSTRACT In recent years, the various Internet of Things (IoT) communication technologies have been researched. The third generation partnership project (3GPP) is dedicated to building the IoT platforms, including NB-IoT, eMTC, and URLLC. However, these platforms cannot adequately meet all the needs of future IoT use cases which are usually broad and beyond cellular. In order to reduce the deployment cost, making the full use of the unlicensed spectrum is strongly appealing to the IoT scenarios. Transform domain communication system (TDCS) is a typical system with spectrum sensing and sharing, and it has unique advantages in supporting multiuser communication in a complex electromagnetic environment. Thus, TDCS is proposed for the IoT massive multiple access scenarios. Previous studies indicate that traditional TDCS has poor BER performance when encountering a large number of users, especially with the near–far effect. To address this, a hybrid clustering TDCS targeting at cognitive IoT applications is proposed to support massive multiple access with the near–far effect. The optimal construction method of the sequence set is also given for the hybrid clustering TDCS. Compared with traditional TDCS, the simulation results show that the proposed system achieves an improvement in multiple access ability, and the system performance can be improved by making a compromise on the number of clusters.

INDEX TERMS IoT, TDCS, spectrum sharing, near–far effect, multiple access.

I. INTRODUCTION

Internet of Things (IoT) is a global network of interconnected objects which are uniquely addressed based on standard communication protocols [1], [2]. IoT interconnects "things" and implements machine-to-machine (M2M) communication, which is a means of data communication between heterogeneous devices without manual intervention [3]. In IoT network, a large number of devices are working and exchanging information simultaneously, thus the communication system should have massive multiple access capability [4], [5]. However, the spectrum scarcity problem and fixed spectrum allocation scheme limit the multiple access capability of current communication systems. Therefore, allocating spectrum resources dynamically and improving the utilization efficiency of the spectrum are key issues IoT. The IoT with spectrum sensing and sharing is called cognitive IoT.

The associate editor coordinating the review of this manuscript and approving it for publication was Min Jia.

Current massive multiple access technologies such as Sparse Coded Multiple Access (SCMA) [6], [7], narrowband Internet of Things (NB-IoT) [8], [9], MIMO-based multiple access [10], etc., are not efficient in spectrum sensing and multiplexing. Thus, these technologies cannot be directly used for cognitive IoT [11], [12]. To address this, a communication system, which meets the requirements of cognitive IoT, is researched below. Transform domain communication system (TDCS) is a promising technology that improves spectrum utilization through dynamic spectrum sensing and spectrum allocation [13]–[16] and is therefore suitable for cognitive IoT. TDCS first obtains spectrum information through spectrum sensing and notching, then a fundamental modulation waveform (FMW) will be generated by utilizing the spectral holes that are not occupied based on spectrum sensing result [17]–[19]. In this way, TDCS realizes dynamic spectrum access and spectrum diversity. In a hardware implementation, TDCS can be implemented based on OFDM structure. This makes the system compatible with existing communication systems [20].

The multiple access of traditional TDCS is achieved by assigning different pseudo-random (PR) sequences to different users, and all users occupy the same available spectrum. The receiver performs multi-user demodulation according to the correlation of the FMWs of different users. In cognitive IoT, the network should be designed with the ability of massive device access. Unfortunately, traditional TDCS accommodates a small number of users due to co-channel interference among different users. For this, the interference cancellation is introduced to reduce co-channel interference. Successive interference cancellation (SIC) is an effective way to improve the performance of TDCS multiple access. However, as the number of users increases, the computation complexity of SIC increases dramatically.

In recent research, a clustering method has been proposed to improve the spectrum utilization efficiency of TDCS [21], [22]. In the case of a small number of clusters, this method hardly affects the BER performance of the system. Thus, it can be applied to improve the multiple access performance of TDCS. In this paper, we are concerned with a transmission scheme in cognitive IoT. In such a scenario, multiple access ability and spectrum utilization efficiency are needed to be considered. Thus, a hybrid clustering TDCS multiple access system is proposed to improve the spectrum utilization efficiency and system performance. Unlike traditional TDCS multiple access systems, the proposed system first allocates the available spectrum to different clusters based on a clustering strategy. Then the same number of users are assigned to each cluster. Since the clusters are orthogonal to each other, the co-channel interference is only from the overlapping users on the same cluster instead of from all other users. For this case, the co-channel interference can be efficiently reduced by applying the SIC receiver. And compared with traditional TDCS, the SIC receiver of hybrid clustering TDCS has a lower computation complexity.

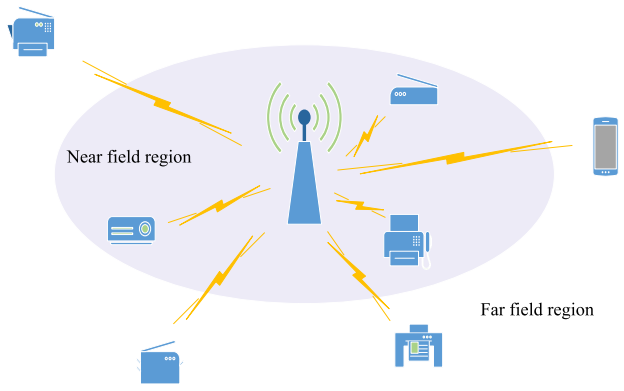

FIGURE 1. Schematic diagram of the near-far effect in the IoT.

Similar to other mobile communication systems, another issue of wireless IoT system is the near-far effect [23]. As shown in Fig. 1, signals from different devices arrive at the base station with different distance and path, which causes the power difference of the signals among the devices. The near-far effect has a large impact on the system capacity and has become an urgent challenge in IoT scenarios. In order to overcome or even exploit this impact, many works on resource allocation, green communication, and SIC has been studied [24], [26].

Since the hybrid clustering TDCS system achieves waveform modulation and the demodulation according to the correlation between the local and received waveforms, considering the near-far effect of IoT and the clustering strategy of TDCS, a lower bound of the correlation function of power difference sequence set with spectral constraint is given in this paper. The lower bound is significant in information theory and can provide some theoretical reference for the cognitive communication/radar waveform design. Based on the lower bound, a construction method of the frequency-domain sequence set is obtained to reduce the interference of TDCS.

It can be summarized that the proposed hybrid clustering TDCS has the following features: 1) Making full use of spectrum resources and supporting spectrum sharing. 2) Providing reliable communication in the case of near-far effect and spectral constraint. 3) Supporting massive access for devices. 4) Simple hardware implementation that can share the hardware structure with traditional OFDM systems.

The rest of this paper is organized as follows. The transmitting and receiving schemes of traditional TDCS are introduced in Section II. The proposed hybrid clustering TDCS is described in Section III. Section IV gives the lower bound of sequences set and corresponding design method. In Section V, numerical simulations are presented. Conclusions are drawn in Section VI.

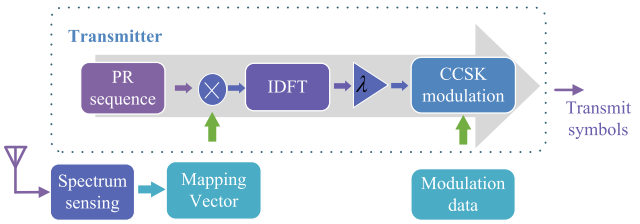

FIGURE 2. The schematic of traditional TDCS transmitter.

II. TRADITIONAL TDCS STRUCTURE

The schematic of TDCS transmitter is shown in Fig. 2. In TDCS, the entire spectrum band is divided into N subcarriers. Then the transmitter conducts spectrum sensing of the electromagnetic environment over the system bandwidth (BW). As shown in Fig. 3, if the subcarriers are occupied, they will be unavailable to TDCS while the transmitted powers in the frequency domain are set to zeros as well. Let $\mathbf{a} = [a_1, a_2, \ldots, a_N]$ denotes the carrier mapping vector, where $a_i = 0$ means the ith subcarrier is unavailable, and $a_i = 1$ means the ith subcarrier is available. Let $\Omega = \{k|a_k = 1\}$ denotes the set of available subcarriers, and N_a is the size

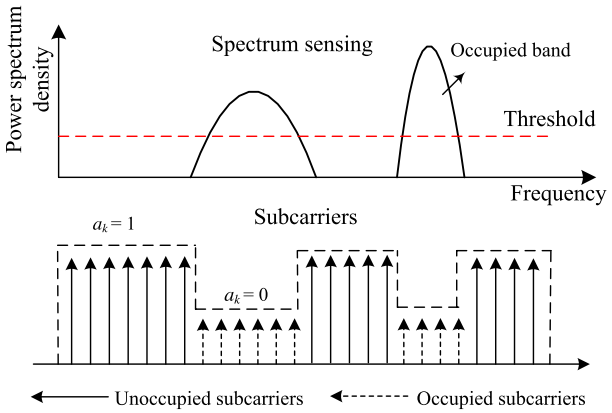

FIGURE 3. The spectrum structure of TDCS.

of Ω. $\bar{\mathbf{\Omega}} = \{0, 1, \ldots, N-1\} \backslash \Omega$ denotes the set of unavailable subcarriers, i.e., $\bar{\mathbf{\Omega}}$ represents the constrained spectrum, and N_s is the size of $\bar{\mathbf{\Omega}}$.

After spectrum sensing and subcarrier mapping, a complex PR phase vector: $\mathbf{q} = [e^{jm_0}, e^{jm_1}, \cdots, e^{jm_{N-1}}]^{\mathrm{T}}$ is generated to get the spectral basic vector $\mathbf{B}$

$$\mathbf{B} = \lambda \cdot diag(\mathbf{a})\mathbf{q}, \tag{1}$$

where $\lambda = \sqrt{N/N_a}$, is an adjustable constant which ensures transmission symbols have the same energy. The FMW, $\mathbf{b}$, can be generated by performing an inverse discrete Fourier transform (IDFT) of $\mathbf{B}$

$$\begin{cases} \mathbf{b} = \mathrm{IDFT}(\mathbf{B}) \\ b_k = \frac{\lambda}{\sqrt{N}} \sum_{n=0}^{N-1} a_k e^{jm_k} e^{j\frac{2\pi kn}{N}}. \end{cases} \tag{2}$$

Then the transmitting data are modulated based on $\mathbf{b}$. Cyclic code shift keying (CCSK) is a form of M_{ary} signaling over a communication channel which modulate data into the cyclic shift version of $\mathbf{b}$: $\mathbf{x} = [x(0), x(1), \cdots, x(N-1)] = \langle \mathbf{b} \rangle_S$, where $\langle \cdot \rangle_S$ denotes the operation of S-point cyclic shift, where S is the transmitting data. By applying CCSK modulation, the transmitting waveform can be expressed as

$$x_k = \frac{\lambda}{\sqrt{N}} \sum_{k=0}^{N-1} a_k e^{jm_k} e^{\frac{j2\pi kn}{N}} e^{\frac{-j2\pi Sk}{M_{ary}}}. \tag{3}$$

The use of the binary sequence as the PR phase vector provides a low probability of intercept for the system. As a soft spreading spectrum technology, CCSK has higher data rate compared to direct spreading spectrum while maintains excellent anti-jamming ability and BER performance as well [27].

As shown in Fig. 4, the receiver structure is compatible with OFDM structure. We assume the carrier mapping vector obtained by spectrum sensing and noticing at the receiver side is identical with that at the transmitter. Prior to signal demodulation, the receiver adopts the same method as the

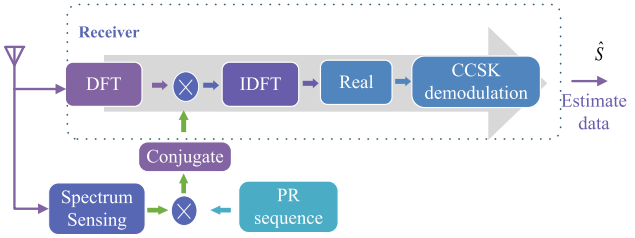

FIGURE 4. The schematic of traditional TDCS receiver.

transmitter to generate a local reference FMW. Note that the power spectrum, i.e., $\left[|B_0|^2, |B_1|^2, \ldots, |B_{N-1}|^2\right]$, and the periodic auto-correlation function is a Fourier transform pair. Thus, the signal processing at the receiver is aim to calculate the auto-correlation of FMW. The transmitted signals have different shift version corresponding to the modulated data, the position of the auto-correlation peak at receiver indicates transmitting data. Since the peak of auto-correlation is the power of FMW which is a real number, the operation of obtaining the real number of auto-correlation can reduce the sidelobes of auto-correlation function without changing the peak value.

After passing an additive white Gaussian noise (AWGN) channel, the received signal can be expressed as

$$r_n = \lambda \frac{1}{\sqrt{N}} \sum_{k=0}^{N-1} a_k e^{jm_k} e^{j\frac{2\pi(n-S)k}{N}} + \omega(n), \tag{4}$$

where $\omega(n)$ denotes the complex-valued AWGN noise with a power density spectrum $\Phi_\omega(f) = N_0$. For detection, the received signal, $\mathbf{r} = [r_0, \ldots, r_{N-1}]$ is correlated with reference FMW to recover input data by detecting the maximum correlation output which can be performed with FFT to minimize computational complexity.

$$\mathbf{y} = \Re\left(\mathrm{IDFT}\left(diag\left((\mathbf{B})^*\right)\mathrm{DFT}(\mathbf{r})\right)\right), \tag{5}$$

where $\Re(\cdot)$ denotes obtaining the real component of a complex number. Then CCSK based demodulation will be applied based on the peak of $\mathbf{y}$.

In traditional TDCS, all users occupy the same frequency band and this causes severe multi-user interference (MUI). Thus, TDCS has poor BER performance when the number of users is large, which is not applicable for IoT massive multiple access. TDCS with SIC receiver can improve the system capacity, however, it results in high complexity of hardware implementation when encountering a large number of users. Thus, a hybrid clustering TDCS is introduced to reduce the complexity and improve system capacity.

III. HYBRID CLUSTERING TDCS SYSTEM MODEL AND CLUSTERING STRATEGIES ANALYSIS

A. HYBRID CLUSTERING TDCS SYSTEM

In this section, a hybrid clustering TDCS is introduced to overcome the drawbacks of TDCS in multiple access. As shown in Fig. 5, after spectrum sensing, the available

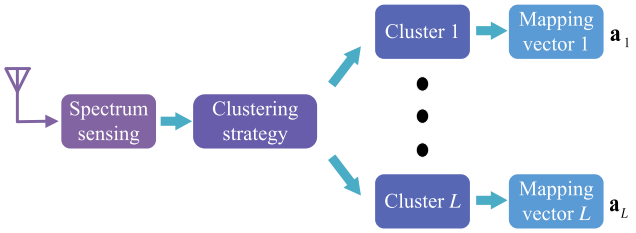

FIGURE 5. Spectrum structures diagram of clustering strategy.

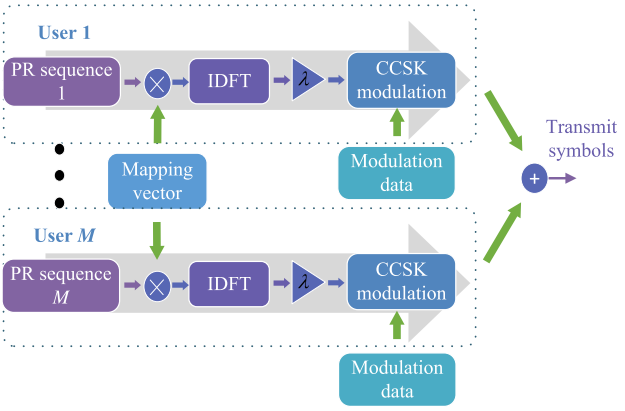

FIGURE 6. Block diagram of the transmitter of lth cluster.

subcarriers are equally divided into L clusters, and each cluster contains N_a/L subcarriers. Note that the clusters are orthogonal to each other

$$\mathbf{\Omega}_{l_1} \cap \mathbf{\Omega}_{l_2} = \mathbf{\Phi}, \quad \bigcup_{l=1}^{L} \mathbf{\Omega}_l = \mathbf{\Omega}, \tag{6}$$

where $\mathbf{\Phi}$ denotes the empty set, $\mathbf{\Omega}_l$ denotes the subcarriers set of lth cluster. Different from the traditional cluster-based TDCS [21] which allocates one user on each cluster, hybrid clustering TDCS can achieve massive multiple access by allocating more users on each cluster. We assume that M users are assigned to each cluster, then the total number of users is $U = ML$. The FMWs of different users are given by $\mathbf{\Omega}_l$ and different PR sequences $\mathbf{q}_m, m = 1, \ldots, M$

$$\mathbf{b}_l^m = \lambda \cdot \mathrm{IDFT}\left(\mathbf{a}_l \cdot \mathbf{q}_m\right), \tag{7}$$

where $\mathbf{b}_l^m$ is the mth FMW on lth cluster, $\mathbf{a}_l$ is the carrier mapping vector of Ω_l and $\cdot$ denotes Hadamard product. After CCSK modulation, the transmitting waveform can be expressed as

$$x_n = \sum_{l=1}^{L} \sum_{m=1}^{M} \sum_{k=0}^{N-1} a_l^k q_m^k e^{\frac{-j2\pi S_l^m k}{M_{ary}}} e^{\frac{j2\pi kn}{N}}, \tag{8}$$

where $S_l^m \in \{1, 2, \ldots, M_{ary}\}$ denotes the data carried by mth FMW on lth cluster.

After passing through AWGN channel, the received waveform $r = [r_0, r_1, \ldots, r_{N-1}]$ can be expressed as

$$r_n = \lambda \sum_{m=1}^{M} \sum_{k=0}^{N-1} \left(\sum_{l=1}^{L} a_l^k q_m^k e^{\frac{-j2\pi S_l^m k}{M_{ary}}} \right) e^{\frac{j2\pi kn}{N}} + w_n, \tag{9}$$

where w_n indicates the noise. Following the CCSK demodulation, the data S_l^m is demodulated by detecting the shift version of the auto-correlation peak, and the signal after passing correlator can be written as

$$\mathbf{y}_l^m = \mathrm{IDFT}\left(\mathrm{DFT}\left(\mathbf{r}\right) \cdot \left(\mathbf{a}_l \cdot \mathbf{q}_m\right)^*\right), \tag{10}$$

where $\mathbf{a}_l \cdot \mathbf{q}_m$ denotes the frequency-domain local reference mth FMW on lth cluster. Utilizing the constraint in (6), the τth element of $\mathbf{y}_l^m$ is derived as

$$\begin{aligned} y_l^m(\tau) = & \overbrace{\sum_{p=0}^{N-1} \lambda \left|a_l^p\right|^2 e^{\frac{-j2\pi S_l^m p}{M_{ary}}} e^{\frac{j2\pi p\tau}{N}}}^{auto-correlation} \\ & + \overbrace{\sum_{p=0}^{N-1} \sum_{\substack{m_1=1 \\ m_1 \neq m}}^{M} \lambda \left|a_l^p\right|^2 q_{m_1}^p \left(q_m^p\right)^* e^{\frac{-j2\pi S_l^{m_1} p}{M_{ary}}} e^{\frac{j2\pi p\tau}{N}}}^{cross-correlation} \\ & + \overbrace{\sum_{p=0}^{N-1} \left(\sum_{n=0}^{N-1} w_n e^{\frac{-j2\pi kn}{N}} \right) \left(a_l^p q_m^p\right)^* e^{\frac{j2\pi p\tau}{N}}}^{noise}. \end{aligned} \tag{11}$$

Then the demodulated data S_l^m is expressed as

$$\begin{aligned} \tilde{S}_l^m &= \arg\max_{\tau} \{\Re\{y_l^m(\tau)\}\} \\ &= \arg\max_{\tau} \{\Re\{R_l^m(\tau) + \sum_{\substack{m_1=1 \\ m_1 \neq m}}^{M} R_l^{mm_1}(\tau) + n_l(\tau)\}\}, \end{aligned} \tag{12}$$

where $R_l^m(\tau)$ denotes the periodic auto-correlation function (PACF) of $\mathbf{b}_l^m$, $R_l^{mm_1}(\tau)$ denotes the periodic cross-correlation function (PCCF) between $\mathbf{b}_l^m$ and $\mathbf{b}_l^{m_1}$, and $n_l(\tau)$ is AWGN noise. Consequently, the receiver of hybrid clustering TDCS is shown in Fig. 7, and data symbols of other users can be recovered by same procedures described above.

Since there is only a single user on each cluster, the traditional cluster-based TDCS has no MUI problem. Proposed hybrid clustering TDCS has MUI shown in (12) which can be canceled by successive interference cancellation (SIC). Therefore, compared with single-user cluster-based TDCS, the proposed system can contain more users when the number of clusters is fixed.

SIC decoding complexity: An important feature of the SIC receiver is its decoding complexity. Based on the special demodulation of CCSK, the demodulation of each user requires an N-point IDFT operation, whose multiplication complexity can be reduced to $N/2\log_2 N$ by inverse fast Fourier transform (IFFT), and N complex multiplication operations, so the multiplication complexity of each SIC

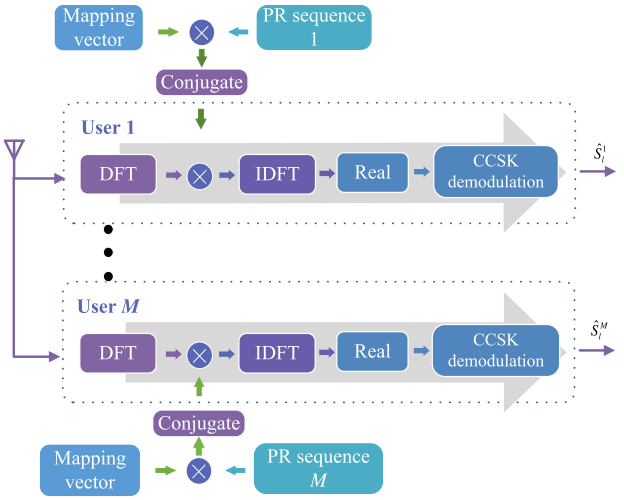

FIGURE 7. Block diagram of the receiver of hybrid clustering TDCS.

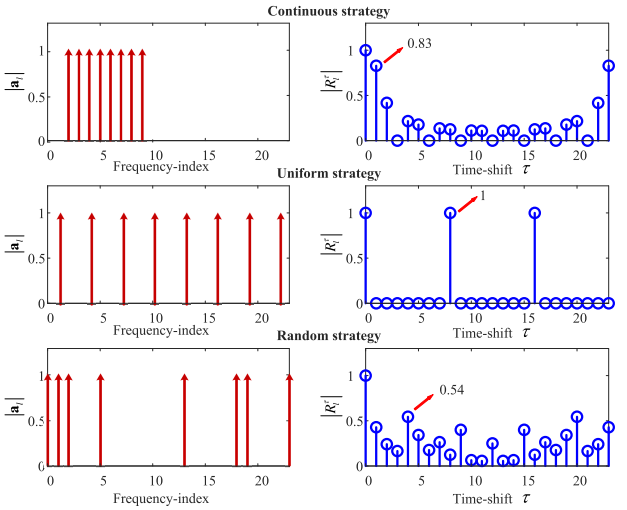

FIGURE 8. Spectrum structures and auto-correlation functions diagram of clustering strategies.

operation is linear with $N\left(\log_2 N+2\right)/2$. And in clustering TDCS, due to divide the all users into L clusters, the complexity on each cluster is linear with $U/L-1$, and the total complexity is linear with $U-L$. In summary, the total SIC decoding complexity of TDCS is $\mathcal{O}((U-L)N\log_2 N)$.

B. CLUSTERING STRATEGIES

As shown in (11), the PACF is related to the carrier mapping vector $\mathbf{a}_l$ and data symbol S_l^m, where S_l^m determines the shift version of PACF, and $\mathbf{a}_l$ determines the value of PACF. We assume $S_l^m = 0$ thus the peak of PACF is at location 0, and other locations are the sidelobes of PACF which interferes with the detection of PACF peak in (12). Therefore, the normalized PACF lobes can be defined as

$$R_l^\tau = \frac{\sum_{p=0}^{N-1}\lambda\left|a_l^p\right|^2 e^{\frac{j2\pi p\tau}{N}}}{\sum_{p=0}^{N-1}\lambda\left|a_l^p\right|^2} = \frac{L}{N_a}\sum_{p=0}^{N-1}\left|a_l^p\right|^2 e^{\frac{j2\pi p\tau}{N}}, \quad (13)$$

where $\tau=0,\ldots,N-1$. In order to detect the peak of PACF efficiently, the objective of clustering strategy is to minimize the sidelobes of PACF: $\left\{R_l^\tau, \tau\neq 0\right\}$. The objective function can be expressed as

$$\begin{aligned}\beta_{\min} &= \min\left\{\max_{l,\tau}\left\{|R_l^\tau|, \tau\neq 0\right\}\right\}\\ s.t. &\quad \bigcup_{l=1,2,\ldots L}\mathbf{\Omega}_l = \mathbf{\Omega}\\ &\quad \bigcap_{l=1,2,\ldots L}\mathbf{\Omega}_l = \mathbf{\Phi}, \end{aligned} \quad (14)$$

According to the Stirling approximation [28], the objective function in (14) is an *NP*-hard problem. There are three typical clustering strategies researched in [21]: continuous strategy, uniform strategy, and random strategy. Fig. 8 shows the spectrum structure and PACF lobes of these three strategies. The observation can be explained as follows: as mentioned above, PACF and the power spectrum is a Fourier transform pair. Thus the PACF and the carrier mapping vector $\mathbf{a}_l$ is almost a Fourier transform pair. Consider the IDFT of $\mathbf{a}_l$ if a continuous strategy is adopted, the PACF is similar to the sinc function which has large sidelobes near the peak. And the smaller occupied subcarriers number is, the larger sidelobes are. If the uniform strategy is adopted, since frequency domain interpolation 0 is equivalent to time domain repetition, PACF has L equal peaks, which can't be used in TDCS. And the random strategy is the best of the three strategies, whose largest sidelobes of PACF is lower than that of the other two strategies. At the same time, the clustering strategy can be optimized through Monte Carlo trials.

However, the random method is almost impossible to get the optimal clustering strategy. In a recent study, a spectrally constrained sequences construction method was given in [29]. The sequences generated by this method have ideal PACF performance. Thus, the clustering strategies based on this method are optimal. However, the construction method is based on the cyclic difference set which can be generated in some specific cases but not generalized, e.g., when N is an even number, the cyclic difference set with the parameter (N,k,λ) does not exist. Therefore, the random clustering strategy is mainly adopted in this paper.

IV. CORRELATION LOWER BOUND OF POWER DIFFERENCE SEQUENCE SET AND WAVEFORM CONSTRUCTION

As discussed above, the multiple access capacity of TDCS system can be improved by allocating the subcarriers to several clusters. However, spectrum clustering will cause the PACF performance deterioration of the sequence, this means that we cannot increase the multiple access capability of TDCS by increasing the number of clusters infinitely. Since the sequence sets of different clusters are orthogonal in

frequency-domain, only the PACF and the PCCF sidelobes of sequences on the same cluster are analyzed in this section.

Let $\mathbf{Y} = [\mathbf{y}_1, \mathbf{y}_2, \ldots, \mathbf{y}_M]^{\mathrm{T}}$ denotes a set of M frequency-domain sequences, where $\mathbf{y}_m = [y_m(0), y_m(1), \ldots, y_m(N-1)]^{\mathrm{T}}$ is a complex-valued sequence of length N. $\mathbf{X} = [\mathbf{x}_1, \mathbf{x}_2, \ldots, \mathbf{x}_M]^{\mathrm{T}}$ denotes the time-domain sequence set corresponding to $\mathbf{Y}$, where $\mathbf{x}_m = \mathbf{F}^{\mathrm{H}}\mathbf{y}_m = [x_m(0), x_m(1), \ldots, x_m(N-1)]^{\mathrm{T}}$, and $\mathbf{F}$ denotes DFT matrix

$$[F]_{mn} = \frac{1}{\sqrt{N}} e^{-j\frac{2\pi mn}{N}}, \quad m, n = 0, \ldots, N-1. \tag{15}$$

The PCCF and the PACF of $\mathbf{X}$ are defined as

$$\begin{cases} r_{x_{m_1}x_{m_1}}(k) = \sum_{n=0}^{N-1} x_{m_1}(n)\, x_{m_1}^*((n-k) \bmod N) \\ r_{x_{m_1}x_{m_2}}(k) = \sum_{n=0}^{N-1} x_{m_1}(n)\, x_{m_2}^*((n-k) \bmod N), \end{cases} \tag{16}$$

where $k = -(N-1), \ldots, (N-1)$, and "mod" is the modulo operator. For simplicity, the PACF of x_m is written as $r_{x_m}(k)$. In order to measure the sidelobes of PACF and PCCF, a metric named sidelobes power sum (SPS) of sequence set $\mathbf{X}$ is defined as

$$\mathrm{SPS} = \underbrace{\sum_{m=1}^{M}\sum_{k=1}^{(N-1)} \left|r_{x_m}(k)\right|^2}_{\mathrm{PACF}} + \underbrace{\sum_{m_1=1}^{M}\sum_{\substack{m_2=1 \\ m_2\neq m_1}}^{M}\sum_{k=0}^{(N-1)} \left|r_{x_{m_1}x_{m_2}}(k)\right|^2}_{\mathrm{PCCF}}, \tag{17}$$

which contains the PACF sidelobes and PCCF sidelobes. In TDCS signal processing, the sidelobes of PACF and PCCF are regarded as interference. Thus, the sequence sets with low SPS metric need to be designed in TDCS. There are two lower bounds of SPS metric without the power difference. When all subcarriers are available and the powers of sequences are set to N, Welch bound is given in [30]: $\mathrm{SPS} \geq N^2M(M-1)$. When a constrained spectrum is considered, the bound of spectrally-constrained sequences is given in [29]: $\mathrm{SPS} \geq N^2M(NM/N_a - 1)$. Furthermore, a lower bound of the sequence set with power difference and the constrained spectrum is given in this section.

The carrier mapping vector $\mathbf{a}$, the available subcarrier set $\mathbf{\Omega}$, and the set of unavailable subcarrier set $\bar{\mathbf{\Omega}}$ are defined in section II, and more definitions are given below. The power of $\mathbf{y}_m$ is defined as $P_m = \sum_{k=0}^{N-1} |y_m(k)|^2$, and $\mathbf{p} = [P_1, P_2, \ldots, P_M]$ denotes the power mapping vector of $\mathbf{Y}$. According to Parsval's theorem, $\mathbf{p}$ is also the power mapping vector of $\mathbf{X}$. Let $\mathbf{X}_m$ denote the right-circulant matrix of $\mathbf{x}_m$

$$\mathbf{X}_m = \begin{bmatrix} x_m(0) & x_m(1) & \ldots & x_m(N-1) \\ x_m(N-1) & x_m(0) & \ldots & x_m(N-2) \\ \vdots & \vdots & \ddots & \vdots \\ x_m(1) & x_m(2) & \ldots & x_m(0) \end{bmatrix}. \tag{18}$$

Clearly every row of $\mathbf{X}_m$ is a cyclically shifted version of the sequence $\mathbf{x}_m$. There is a well-known conclusion

$$\mathbf{X}_m = \mathbf{F}^{\mathrm{H}}\mathbf{Y}_m\mathbf{F}, \tag{19}$$

where $\mathbf{Y}_m = \sqrt{N}\,diag(\mathbf{y}_m)$ which is proved in [31]. Then all the $\mathbf{X}_m$ are stacked together

$$\hat{\mathbf{X}}^{\mathrm{T}} = \left[\mathbf{X}_1^{\mathrm{T}}, \mathbf{X}_2^{\mathrm{T}}, \ldots, \mathbf{X}_M^{\mathrm{T}}\right]_{N\times MN}. \tag{20}$$

The correlation matrix of $\mathbf{X}$ can be expressed as

$$\mathbf{R} = \hat{\mathbf{X}}\hat{\mathbf{X}}^{\mathrm{H}} = \begin{bmatrix} \mathbf{R}_{11} & \mathbf{R}_{12} & \ldots & \mathbf{R}_{1M} \\ \mathbf{R}_{21} & \mathbf{R}_{22} & \ldots & \mathbf{R}_{2M} \\ \vdots & \vdots & \ddots & \vdots \\ \mathbf{R}_{M1} & \mathbf{R}_{M2} & \ldots & \mathbf{R}_{MM} \end{bmatrix}. \tag{21}$$

where $\mathbf{R}_{m_1m_2}, m_1, m_2 = 1, 2, \ldots, M$, denotes the correlation matrix of $\mathbf{x}_{m_1}$ and $\mathbf{x}_{m_2}$

$$\mathbf{R}_{m_1m_2} = \begin{bmatrix} r_{x_{m_1}x_{m_2}}(0) & r_{x_{m_1}x_{m_2}}(1) & \ldots & r_{x_{m_1}x_{m_2}}(N-1) \\ r_{x_{m_1}x_{m_2}}^*(N-1) & r_{x_{m_1}x_{m_2}}(0) & \ldots & r_{x_{m_1}x_{m_2}}(N-2) \\ \vdots & \vdots & \ddots & \vdots \\ r_{x_{m_1}x_{m_2}}^*(1) & r_{x_{m_1}x_{m_2}}^*(2) & \cdots & r_{x_{m_1}x_{m_2}}(0) \end{bmatrix}. \tag{22}$$

Observed from (21) and (22), the matrix $\mathbf{R}_{mm}$ on the main diagonal is auto-correlation matrix of $\mathbf{x}_m$, and the peak of PACF is $r_{x_mx_m}(0) = P_m$. Therefore, the power mapping vector $\mathbf{p}$ is considered in the time-domain sequence set $\mathbf{X}$. Note that each PACF and PCCF value appears N times in correlation matrixes, the SPS of $\mathbf{X}$ can be represented as

$$\begin{aligned} \mathrm{SPS} &= \frac{1}{N}\left\|\mathbf{R} - \mathbf{D}_p\right\|^2 \\ \mathbf{D}_p &= diag(\mathbf{p}) \otimes \mathbf{I}_N, \end{aligned} \tag{23}$$

where $\otimes$ denotes the Kronecker product operation and $\|\cdot\|$ denotes the Frobenius norm of a matrix. For simplifying the problem (23), we define

$$\begin{aligned} \tilde{\mathbf{F}} &= \begin{bmatrix} \mathbf{F} & & \mathbf{0} \\ & \ddots & \\ \mathbf{0} & & \mathbf{F} \end{bmatrix}_{MN\times MN} \\ \mathbf{Q}^{\mathrm{T}} &= \left[\mathbf{Y}_1^{\mathrm{T}}, \mathbf{Y}_2^{\mathrm{T}}, \ldots, \mathbf{Y}_M^{\mathrm{T}}\right], \end{aligned} \tag{24}$$

where $\tilde{\mathbf{F}}$ is an unitary matrix: $\tilde{\mathbf{F}}\tilde{\mathbf{F}}^{\mathrm{H}} = \mathbf{I}_{MN\times MN}$. Based on (19) and (24), the SPS in (23) can be rewritten as

$$\mathrm{SPS} = \frac{1}{N}\left\|\tilde{\mathbf{F}}^{\mathrm{H}}\mathbf{Q}\mathbf{Q}^{\mathrm{H}}\tilde{\mathbf{F}} - \mathbf{D}_p\right\|^2 = \frac{1}{N}\left\|\mathbf{Q}\mathbf{Q}^{\mathrm{H}} - \mathbf{D}_p\right\|^2. \tag{25}$$

As shown in (25), the SPS metric of $\mathbf{X}$ is connected with the frequency-domain sequence set $\mathbf{Y}$ and the power mapping vector $\mathbf{p}$. Then the spectral constraint $\bar{\Omega}$ is considered, where $y_m(p) = 0, \forall\, p \in \bar{\Omega}$, and we define

$$\mathbf{z}_p = \sqrt{N} \cdot [y_1(p), y_2(p), \ldots, y_M(p)]^{\mathrm{T}}, \tag{26}$$

where $p \in \{0, \ldots, N-1\}$. Thus, (25) can be rewritten as

$$\begin{aligned} \mathrm{SPS} &= \frac{1}{N} \sum_{\substack{p=1 \\ p \in \Omega}}^{M} \left\| \mathbf{z}_p \mathbf{z}_p^{\mathrm{H}} - diag\left(\mathbf{p}\right) \right\|^2 + \frac{N_s}{N} \sum_{m=1}^{M} P_m^2 \\ &= \frac{1}{N} \widetilde{\mathrm{SPS}} + \frac{N_s}{N} \sum_{m=1}^{M} P_m^2, \end{aligned} \tag{27}$$

where P_m is the power of $\mathbf{y}_m$. (27) can be further rewritten as

$$\begin{aligned} \widetilde{\mathrm{SPS}} &= \sum_{\substack{p=0 \\ p \in \Omega}}^{N-1} tr\left[\left(\mathbf{z}_p \mathbf{z}_p^{\mathrm{H}} - diag\left(\mathbf{p}\right) \right) \left(\mathbf{z}_p \mathbf{z}_p^{\mathrm{H}} - diag\left(\mathbf{p}\right) \right)^{\mathrm{H}} \right] \\ &= \sum_{\substack{p=0 \\ p \in \Omega}}^{N-1} \left(\left\| \mathbf{z}_p \right\|^4 - 2 \left\| diag\left(\sqrt{\mathbf{p}}\right) \mathbf{z}_p \right\|^2 \right) + N_a \sum_{m=1}^{M} P_m^2 \\ &\geq \sum_{\substack{p=0 \\ p \in \Omega}}^{N-1} \left(\left\| \mathbf{z}_p \right\|^4 - 2 \sqrt{ \sum_{m=1}^{M} P_m^2 \sum_{m=1}^{M} \left| z_p\left(m\right) \right|^4 } \right) \\ &\quad + N_a \sum_{m=1}^{M} P_m^2 = \widehat{\mathrm{SPS}} + N_a \sum_{m=1}^{M} P_m^2, \end{aligned} \tag{28}$$

where $\mathrm{SPS} \geq \frac{1}{N} \widehat{\mathrm{SPS}} + \sum_{m=1}^{M} P_m^2$. According to Cauchy-Schwarz inequality, the equality is achieved if and only if

$$\frac{\left| z_1\left(p\right) \right|}{\sqrt{P_1}} = \frac{\left| z_2\left(p\right) \right|}{\sqrt{P_2}} = \ldots = \frac{\left| z_M\left(p\right) \right|}{\sqrt{P_M}}, \tag{29}$$

(29) indicates that the power of $\mathbf{Y}$ in same subcarriers are proportional to the power mapping vector $\mathbf{p}$. Note that

$$\sum_{m=1}^{M} \sum_{\substack{p=0 \\ p \in \Omega}}^{N-1} \left| z_m\left(p\right) \right|^2 = N \sum_{m=1}^{M} P_m, \tag{30}$$

therefore, (28) can be further minimized as

$$\begin{aligned} \widehat{\mathrm{SPS}} &\geq \sum_{\substack{p=0 \\ p \in \Omega}}^{N-1} \left(\frac{N}{N_a} \sum_{m=1}^{M} P_m \right)^2 - \frac{\sum_{\substack{p=0 \\ p \in \Omega}}^{N-1} 2 \sum_{m=1}^{M} N P_m^2}{N_a} \\ &= \frac{N^2}{N_a} \left(\sum_{m=1}^{M} P_m \right)^2 - 2N \sum_{m=1}^{M} P_m^2, \end{aligned} \tag{31}$$

where the equality is achieved if and only if

$$\left\| \mathbf{z}_p \right\|^2 = \frac{N}{N_a} \sum_{m=1}^{M} P_m, \quad \forall p \in \Omega, \tag{32}$$

(32) implies that the sum of powers on each subcarrier is equal. Based on (29) and (32), we have

$$\left| y_m\left(p\right) \right|^2 = \frac{P_m}{N_a}, \tag{33}$$

which means that the frequency-domain sequence $\mathbf{y}_m$ is unimodular on occupied subcarriers. In the case of this value, as shown in (31), the lower bound of and spectrum constrained sequence set with power difference can be obtained

$$\mathrm{SPS} \geq \frac{N}{N_a} \left(\sum_{m=1}^{M} P_m \right)^2 - \sum_{m=1}^{M} P_m^2, \tag{34}$$

Remark 1: Consider the frequency-domain sequence set $\mathbf{Y}$ without power difference: $P_m = N, \forall\, m = 1, 2, \ldots, M$. If all subcarriers are available: $N_s = 0$, the lower bound in (34) is equal to the Welch bound: $N^2 M\left(M-1\right)$. If some subcarriers are unavailable: $N_a = N - N_s$, the lower bound in (34) is equal to the bound proposed in [29]: $N^2 M\left(NM/N_a - 1\right)$. Therefore, the lower bound given in (34) is generalized.

Remark 2: Let us discuss the conditions for the equal sign in inequalities (28) and (31). When sequence set $\mathbf{Y}$ without the power difference: $diag\left(p\right) = N\mathbf{I}_M$, $\sum_{p=0}^{N-1} \left\| \mathbf{z}_p \right\|^2 = MN^3$, the inequality in (28) becomes an equality. Thus, only the inequality in (31) is valid. When the power difference is considered, the inequalities (28) and (31) are both used to obtain the lower bound. These two conditions give the construction methods of the sequence set to reach the lower bounds: For a sequence set design without power difference, the sum of the powers of each subcarrier is equal, and for a sequence set design with power differences, all frequency domain sequences are unimodular on the available subcarriers.

Example 1: Consider the frequency sequence sets with spectral constraint and power difference, where $N = 256$, $N_a = 128$, $M = 3$ and $\mathbf{p} = [N, 2N, 3N]$. There are three type of sequence set: random sequences set generated by time-domain random phase sequences, the semi-optimized sequence set generated based on (32), and the optimal sequence set generated by (33). The SPSs of these sequence sets are given in TABLE 1.

TABLE 1. Values of SPS for random, semi-optimized and optimal sequence sets.

Sequence set type	SPS
Random phase	6105537
Semi-optimized	4017369
Optimal	3801088

In summary, the sequence set design method is given to reach the lower bound of the correlation function in (33). Furthermore, the sequence set with low PAPR can be designed by Gerchberge-Saxton algorithm (GSA) [32] with the spectral modulus constraint of (33), and the idea of the algorithm is simply given as follows.

Let $\mathbf{Y}_{N \times M}$ denote the frequency sequence set that satisfies the spectral constraint $\bar{\Omega}$ and the modular limitation in (33), $\mathbf{V}$ represent an auxiliary variable matrix used to meet the low PAPR requirement, and the optimization problem can be

written as

$$\begin{aligned} \min_{\mathbf{Y},\mathbf{V}} \quad & u(\mathbf{Y},\mathbf{V}) = \left\| \mathbf{F}^{\mathrm{H}}\mathbf{Y} - \mathbf{V} \right\|^2 \\ s.t. \quad & |y_m(p)| = \sqrt{\frac{P_m}{N_a}}, \quad p \in \Omega \\ & |y_m(p)| = 0, \quad p \in \bar{\Omega} \\ & |v_{nm}| = \sqrt{\frac{P_m}{N}}, \end{aligned} \tag{35}$$

where $\mathbf{F}$ denotes the DFT matrix. Due to $\left\|\mathbf{F}^{\mathrm{H}}\mathbf{Y} - \mathbf{V}\right\|^2 = \|\mathbf{Y} - \mathbf{F}\mathbf{V}\|^2$, we have: $u\left(\mathbf{Y}^k, \mathbf{V}^k\right) \geq \min_{\mathbf{V}} \left\|\mathbf{F}^{\mathrm{H}}\mathbf{Y}^k - \mathbf{V}\right\|^2 = u\left(\mathbf{Y}^k, \mathbf{V}^{k+1}\right) \geq \min_{\mathbf{Y}} \left\|\mathbf{Y} - \mathbf{F}\mathbf{V}^{k+1}\right\|^2 = u\left(\mathbf{Y}^{k+1}, \mathbf{V}^{k+1}\right)$. By using the GSA algorithm, the low PAPR algorithm for spectral constraint sequence set is given as follows

Step 0: Give the initial random phase sequence sets $\mathbf{Y}^0$ and $\mathbf{V}^0$ satisfy the constraint in (34).

Step 1: Fix $\mathbf{Y}^k$, compute the IDFT of $\mathbf{Y}^k$, the optimal $\mathbf{V}^{k+1}$ is given by: $\mathbf{V}^{k+1} = \arg\left(u\left(\mathbf{Y}^k, \mathbf{V}\right)\right)$.

Step 2: Fix $\mathbf{V}^{k+1}$, compute the DFT of $\mathbf{V}^{k+1}$, the optimal $\mathbf{Y}^{k+1}$ is given by: $\mathbf{Y}^{k+1} = \arg\left(u\left(\mathbf{Y}, \mathbf{V}^{k+1}\right)\right)$.

Iteration: repeat steps 1 and 2, until a pre-specified stop condition is met.

V. SIMULATION RESULTS

In this section, we assume the spectrum BW is $W = 10$ MHz, the occupied spectrum bands are set in the range 1.25-2.5 MHz and 7.5-8.75 MHz. Thus, the ratio of the available spectrum band to the entire BW is $\beta = 3/4$. E_b is the energy per bit of the transmitting signal, and E_b/N_0 is the energy per bit to noise power spectral density ratio in dB. More simulation parameters are shown in TABLE 2, where P_u is the power of user u and is randomly selected from 0-5/0-10 dB. The power estimation of the SIC receiver is considered to be ideal and the BER performance of the user with minimal power is given in the following simulation.

TABLE 2. Simulation parameters.

Parameters	Symbol	Value
Number of subcarriers	N	256
Available subcarriers	N_a	192
Value of powers	P_u	0-5/0-10 (dB)
Number of users	U	16/32
Number of clusters	L	1/8/16/32
Modulation order of CCSK	M_{ary}	256

A. BER PERFORMANCE SIMULATION IN AWGN CHANNEL

Fig. 9 shows the BER performance of TDCS with different L in an AWGN channel, where U is fixed to 16. Comparing the BER performance of TDCS with different $L = 16, 8, 4, 1$, the BER performance increases as L decreases. On the other hand, the complexity of the SIC receiver increases with a decrease of L. Therefore, there is a tradeoff of L between BER performance and the complexity of the SIC receiver when a small U is chosen.

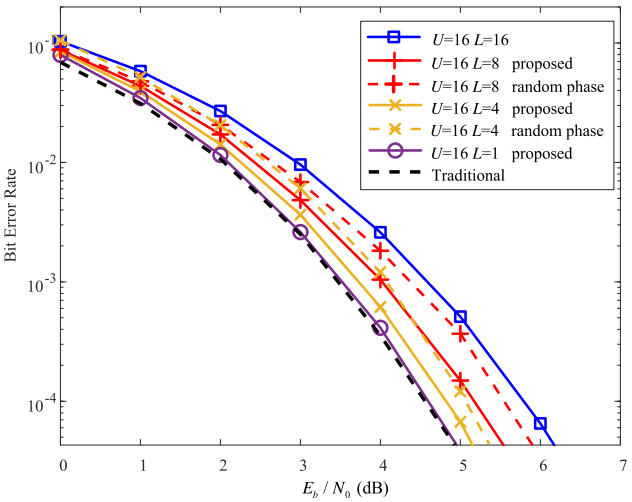

FIGURE 9. BER performance comparison of TDCS with $L = 1, 4, 8, 16$ for $U = 16$ ($N = 256$, $P_u \in [0, 10]$).

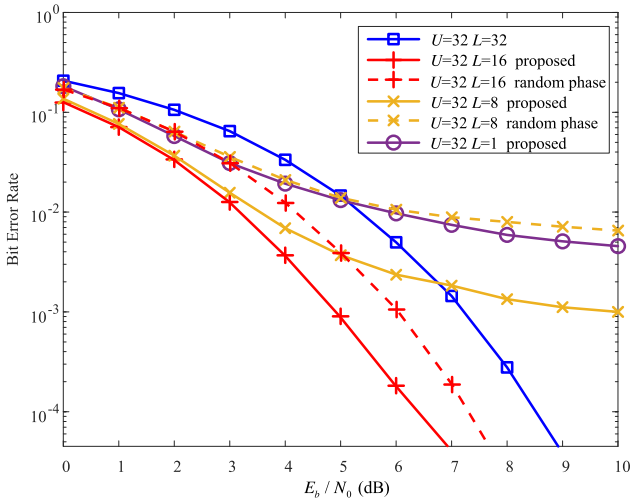

FIGURE 10. BER performance comparison of TDCS with $L = 1, 8, 16, 32$ for $U = 32$ ($N = 256$, $P_u \in [0, 10]$).

However, as U increases, the conclusion does not always apply. As shown in Fig. 10, when the small L is adopted for $U = 32$ ($L = 1, 8$), due to the severe MUI caused by overlapping excessive users on the same cluster and the PACF distortion caused by large L, some special CCSK shift versions are covered by interference. Therefore, it is difficult for the SIC receiver to effectively reduce the MUI, and E_b/N_0-BER curve converges to a flat/poor state. However, the TDCS with large L still maintains excellent BER performance ($L = 16, 32$) due to small MUI. This observation suggests that when the large U is considered, L should be carefully selected to improve the performance of TDCS.

Furthermore, the BER performance comparison of the proposed sequence set and random phase sequence set in TDCS

is also given in Fig. 9 and Fig. 10, where the dashed lines indicate the BER performance of TDCS using the random phase sequence set. Since the correlation function sidelobes are reduced by the method proposed in Section IV, in other words, the MUI is suppressed, the proposed sequence set achieves better TDCS BER performance than the random phase sequence set. In particular, when small L for large U is considered (e.g., $U = 32$, $L = 8$). the TDCS using the proposed sequence set has a great BER performance improvement. Therefore, the proposed sequence set is used in the following simulations.

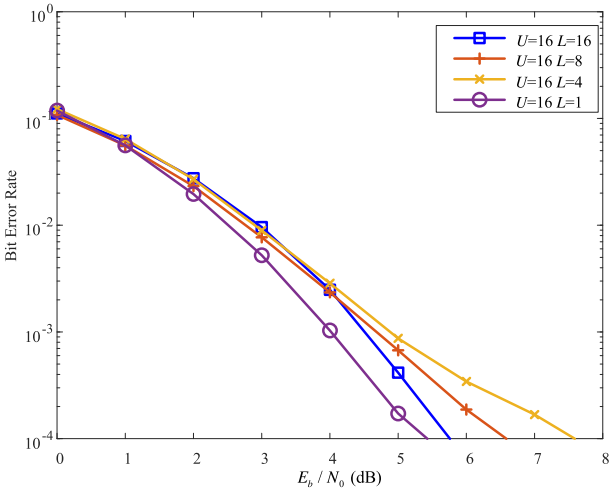

FIGURE 11. BER performance with small power difference ($N = 256$, $P_u \in [0, 5]$, $L = 4$ for $U = 16$ and $L = 8$ for $U = 32$).

To demonstrate the impact of the near-far effect of SIC receiver, Fig. 11 shows the BER performance with $P_u \in [0, 5]$. Compared with Fig. 9, when the same simulation parameters are adopted ($L = 1, 4, 8, 16$ for $U = 16$), the hybrid clustering TDCS with large power difference outperforms that with small power difference ($P_u \in [0, 5]$). When $L = 4$ and $U = 16$, the TDCS with $P_u \in [0, 10]$ achieves a 3 dB gain in terms of E_b/N_0 compared to that with $P_u \in [0, 5]$. This observation indicates that the SIC receiver can achieve performance gains in IoT scenarios with the near-far effect. The TDCS with a single user on each cluster cannot use SIC receiver to improve the multiple access capability of the system. However, observed from Fig. 11 and Fig. 9, it is most stable, i.e., the near-far effect hardly affects its BER performance.

B. BER PERFORMANCE SIMULATION IN MULTIPATH FADING CHANNEL

Let us discuss the BER performance of hybrid clustering TDCS in multipath fading channel (Extended Typical Urban model in [33]). To compact the effect from the multipath fading channel, the cyclic prefix of length $N/4$ and the ideal channel estimation are simulated.

Fig. 12 shows the BER performance of hybrid clustering TDCS with same U and different L in multipath

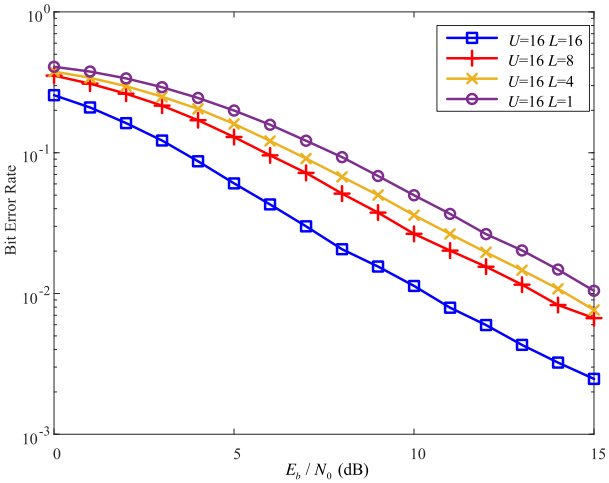

FIGURE 12. BER performance of TDCS with $L = 1, 4, 8, 16$ for $U = 16$ in multipath fading channels ($N = 256$, $P_u \in [0, 10]$).

fading channel. The observation shows that the BER performance deteriorates with the decrease of the L, e.g., when BER $= 10^{-2}$, the performance of 16-cluster TDCS is about 5 dB better than that of traditional single-cluster TDCS in terms of E_b/N_0. Compared with the TDCS with small L, the TDCS with large L occupies fewer subcarriers. Therefore, the hybrid clustering TDCS with large L achieves better BER performance than that with small L, due to avoid the continuous frequency selective fading.

According to the BER performance of hybrid clustering TDCS in AWGN and multipath fading channels, the main conclusions are as shown follows. To achieve better BER performance in AWGN, when $U \leq 20$, L should take small value. However, in order to reduce the complexity of the SIC receiver, the cluster number should be as large as possible. In particular, when $L = U$, the system does not require a SIC receiver. When $U = 32$, TDCS with small L has poor BER performance thus L should be carefully selected. In multipath fading channels, TDCS with large L achieves better performance than traditional single-cluster TDCS. Therefore, the hybrid clustering TDCS can improve multiple access capability and reduce complexity. And in some cases, hybrid clustering TDCS requires a compromise between the BER performance and the complexity of the SIC receiver.

VI. CONCLUSION

In this paper, the wireless communication system which is suitable for cognitive IoT spectrum sharing requirements is investigated. Based on the traditional spectrum sharing system TDCS, a hybrid clustering TDCS multiple access model is proposed to reduce the complexity of SIC receivers by clustering. At the same time, we also consider the near-far effect of the IoT and improve the performance of the SIC receiver by properly allocating users. Based on the spectral constraint and the power difference scene caused by the near-far effect, the lower bound of the power difference sequence set under

spectrum limitation is given, and the design method is given to reach the lower bound. Finally, simulation results confirm that the hybrid clustering TDCS can address the problems caused by the near-far effect and multiple access. This implies that the system can be applied to future cognitive IoT.

REFERENCES

[1] C. Perera, A. Zaslavsky, P. Christen, and D. Georgakopoulos, "Context aware computing for the Internet of Things: A survey," *IEEE Commun. Surveys Tuts.*, vol. 16, no. 1, pp. 414–454, 1st Quart., 2014.
[2] R. Han, Y. Gao, C. Wu, and D. Lu, "An effective multi-objective optimization algorithm for spectrum allocations in the cognitive-radio-based Internet of Things," *IEEE Access*, vol. 6, pp. 12858–12867, 2018.
[3] G. A. Akpakwu, B. J. Silva, G. P. Hancke, and A. M. Abu-Mahfouz, "A survey on 5G networks for the Internet of Things: Communication technologies and challenges," *IEEE Access*, vol. 6, pp. 3619–3647, Dec. 2018.
[4] W. Lu, Y. Gong, X. Liu, J. Wu, and H. Peng, "Collaborative energy and information transfer in green wireless sensor networks for smart cities," *IEEE Trans. Ind. Informat.*, vol. 14, no. 4, pp. 1585–1593, Apr. 2018.
[5] S. Hu, B. Yu, C. Qian, Y. Xiao, Q. Xiong, C. Sun, and Y. Gao, "Nonorthogonal interleave-grid multiple access scheme for industrial Internet of things in 5G network," *IEEE Trans. Ind. Informat.*, vol. 14, no. 12, pp. 5436–5446, Dec. 2018.
[6] H. Nikopour and H. Baligh, "Sparse code multiple access," in *Proc. IEEE 24th Annu. Int. Symp. Pers., Indoor, Mobile Radio Commun.*, Sep. 2013, pp. 332–336.
[7] M. Zhao, S. Zhou, W. Zhou, and J. Zhu, "An improved uplink sparse coded multiple access," *IEEE Commun. Lett.*, vol. 21, no. 1, pp. 176–179, Jan. 2017.
[8] Y.-P. E. Wang, X. Lin, A. Adhikary, A. Grovlen, Y. Sui, Y. Blankenship, J. Bergman, and H. S. Razaghi, "A primer on 3GPP narrowband Internet of Things," *IEEE Commun. Mag.*, vol. 55, no. 3, pp. 117–123, Mar. 2017.
[9] M. Jia, Z. Yin, Q. Guo, G. Liu, and X. Gu, "Downlink design for spectrum efficient IoT network," *IEEE Internet Things J.*, vol. 5, no. 5, pp. 3397–3404, Oct. 2018.
[10] T. E. Bogale and L. B. Le, "Massive MIMO and mmWave for 5G wireless HetNet: Potential benefits and challenges," *IEEE Veh. Technol. Mag.*, vol. 11, no. 1, pp. 64–75, Mar. 2016.
[11] S. Hu, H. Guo, C. Jin, Y. Huang, B. Yu, and S. Li, "Frequency-domain oversampling for cognitive CDMA systems: Enabling robust and massive multiple access for Internet of Things," *IEEE Access*, vol. 4, pp. 4583–4589, 2016.
[12] X. Liu, M. Jia, Z. Na, W. Lu, and F. Li, "Multi-modal cooperative spectrum sensing based on dempster-shafer fusion in 5G-based cognitive radio," *IEEE Access*, vol. 6, pp. 199–208, 2018.
[13] C. Han, J. Wang, Y. Yang, and S. Li, "Addressing the control channel design problem: OFDM-based transform domain communication system in cognitive radio," *Comput. Netw.*, vol. 52, no. 4, pp. 795–815, Mar. 2008.
[14] S. Hu, G. Bi, Y. L. Guan, and S. Li, "Spectrally efficient transform domain communication system with quadrature cyclic code shift keying," *IET Commun.*, vol. 7, no. 4, pp. 382–390, Mar. 2013.
[15] S. Hu, G. Bi, Y. L. Guan, and S. Li, "TDCS-based cognitive radio networks with multiuser interference avoidance," *IEEE Trans. Commun.*, vol. 61, no. 12, pp. 4828–4835, Dec. 2013.
[16] S. Hu, Z. Liu, Y. L. Guan, W. Xiong, G. Bi, and S. Li, "Sequence design for cognitive CDMA communications under arbitrary spectrum hole constraint," *IEEE J. Sel. Areas Commun.*, vol. 32, no. 11, pp. 1974–1986, Nov. 2014.
[17] C. Han, J. Wang, S. Gong, and S. Li, "Detection and performance of the OFDM-based transform domain communication system," in *Proc. Int. Conf. Commun. Circuits Syst.*, Jun. 2006, pp. 1332–1336.
[18] C. Yin, Y. Zheng, D. Ma, G. Yu, and J. Wang, "Detection of the CDMA-based transform domain communication system," in *Proc. IEEE Int. Conf. Wireless Commun. Net. Inf. Secur.*, Jun. 2010, pp. 193–197.
[19] G. M. Dillard, M. Reuter, J. Zeiddler, and B. Zeidler, "Cyclic code shift keying: A low probability of intercept communication technique," *IEEE Trans. Aerosp. Electron. Syst.*, vol. 39, no. 3, pp. 786–798, Jul. 2003.
[20] S. Hu, Q. Luo, F. Li, Z. Liu, Y. Gao, and J. Wu, "Practical implementation of multi-user transform domain communication system for control channels in cloud-based cognitive radio networks," *IEEE Access*, vol. 6, pp. 17010–17021, 2018.
[21] S. Hu, Y. L. Guan, G. Bi, and S. Li, "Cluster-based transform domain communication systems for high spectrum efficiency," *IET Commun.*, vol. 6, no. 16, pp. 2734–2739, Nov. 2012.
[22] Z. Na, Y. Wang, X. Li, J. Xia, X. Liu, M. Xiong, and W. Lu, "Subcarrier allocation based simultaneous wireless information and power transfer algorithm in 5G cooperative OFDM communication systems," *Phys. Commun.*, vol. 29, pp. 164–170, Aug. 2018.
[23] M. Jia, X. Gu, Q. Guo, W. Xiang, and N. Zhang, "Broadband hybrid satellite-terrestrial communication systems based on cognitive radio toward 5G," *IEEE Wireless Commun.*, vol. 23, no. 6, pp. 96–106, Dec. 2016.
[24] T. Lv, Y. Ma, J. Zeng, and P. T. Mathiopoulos, "Millimeter-wave noma transmission in cellular M2M communications for Internet of Things," *IEEE Internet Things J.*, vol. 5, no. 3, pp. 1989–2000, Jun. 2018.
[25] X. Liu, X. Zhang, M. Jia, L. Fan, W. Lu, and X. Zhai, "5G-based green broadband communication system design with simultaneous wireless information and power transfer," *Phys. Commun.*, vol. 28, pp. 130–137, Jun. 2018.
[26] T. Lv, Z. Lin, P. Huang, and J. Zeng, "Optimization of the energy-efficient relay-based massive IoT network," *IEEE Internet Things J.*, vol. 5, no. 4, pp. 3043–3058, Aug. 2018.
[27] S. Hu, F. Li, H. Guo, P. Wang, Y. Gao, Z. Liu, and B. Yu, "TDCS-IDMA system for cognitive radio networks with cloud," *IEEE Access*, vol. 6, pp. 20520–20530, 2018.
[28] D. Romik, "Stirling's approximation for n!: The ultimate short proof?" *Amer. Math. Monthly*, vol. 107, no. 6, pp. 556–557, Jun. 2000.
[29] Z. Liu, Y. L. Guan, U. Parampalli, and S. Hu, "Spectrally-constrained sequences: Bounds and constructions," *IEEE Trans. Inf. Theory*, vol. 64, no. 4, pp. 2571–2582, Apr. 2018.
[30] L. Welch, "Lower bounds on the maximum cross correlation of signals (Corresp.)," *IEEE Trans. Inf. Theory*, vol. 20, no. 3, pp. 397–399, May 1974.
[31] H. He, J. Li , and P. Stoica, *Waveform Design for Active Sensing Systems: A Computational Approach*. Gainesville, FL, USA: Univ. of Florida, 2011.
[32] R. W. Gerchberg and A. W. O. Saxton, "A practical algorithm for the determination of phase from image and diffraction plane pictures," *Optik*, vol. 35, no. 2, pp. 237–250, 1971.
[33] *Evolved Universal Terrestrial Radio Access (E-UTRA); Base Station (BS) Radio Transmission and Reception, Version 11.1.0*, document 3GPP TS36.104, Jul. 2012.

SHIYONG MA received the B.S. degree in basic science of mathematics and physics from the University of Electronic Science and Technology of China, Chengdu, China, in 2017. He is currently pursuing the M.S. degree with the National Key Laboratory of Science and Technology on Communication. His research interests include wireless communication, waveform design, and integrated communication and radar system.

SU HU received the M.S. and Ph.D. degrees from the National Key Laboratory on Communications, University of Electronic Science and Technology of China (UESTC), in 2007 and 2010, respectively. From 2011 to 2012, he was a Research Fellow with the School of Electrical and Electronic Engineering, Nanyang Technological University, Singapore. He is currently a Professor with UESTC. His research interests include sequence design with good correlation properties and physical layer design for wireless communication systems, such as filterbank multicarrier systems and cognitive radio networks.

XUEZHANG ZHU received the bachelor's degree in electrical and information engineering from Southwest Jiaotong University, China, in 2018. He is currently pursuing the master's degree in electronics and communication engineering with the University of Electronic Science and Technology of China. His research interests include machine learning, network protocol, and network fault detection.

QIUDI TANG received the B.S. degree in measuring and controlling technology and instrument from Jilin University, in 2018. She is currently pursuing the master's degree in communication and information system with the University of Electronic Science and Technology of China, Chengdu, China. Her research interests include transform domain communication systems (TDCS) and non-continuous orthogonal frequency division multiplexing (NC-OFDM) systems.

QU LUO received the bachelor's degree from the Chongqing University of Posts and Telecommunications, China, in 2016. He is currently pursuing the master's degree with the National Key Laboratory of Science and Technology on Communication, University of Electronic Science and Technology of China. His research interests include wireless communication, cognitive radio networks, and machine learning.

YUNFENG ZHOU received the B.S. degree in electronic information engineering from Southwest Jiaotong University, in 2018. He is currently pursuing the master's degree in communication and information system with the University of Electronic Science and Technology of China, Chengdu, China. His research interests include network communications, the network fault diagnosis, and machine learning.